Interparticle interaction and crossover in critical lines on field-temperature plane in $Pr_{0.5}Sr_{0.5}MnO_3$ nanoparticles

A. K. Pramanik* and A. Banerjee
UGC-DAE Consortium for Scientific Research, University Campus, Khandwa Road, Indore 452001, Madhya Pradesh, India
(Received 8 June 2010; published 1 September 2010)

The magnetic properties and the effects of interparticle interaction on them have been studied in nanoparticles of half-doped $Pr_{0.5}Sr_{0.5}MnO_3$. Three samples consisting of nanoparticles of different average particle sizes are synthesized to render the variation in interparticle interaction. Though all the samples crystallize in the same structure to that of their bulk compound, the low-temperature ferromagnetic-antiferromagnetic transition, which is present in bulk compound, is not evident in the nanoparticles. Linear as well as nonlinear ac susceptibility coupled with dc magnetic measurements have shown the superparamagnetic behavior of these nanoparticles where the blocking temperature increases with the increasing particle size. Presence of interparticle interaction is confirmed from the temperature variation in coercive field and the analysis of frequency-dependent ac susceptibility. We have identified the nature of this interaction to be of dipolar type and show that its strength decreases with the increasing particle size. The effect of this dipolar interaction on magnetic properties is intriguing as the compounds exhibit crossover from de Almeida-Thouless- to Gabay-Toulouse-type critical lines on field-temperature plane above their respective interaction field. In agreement with theoretical prediction, we infer that this crossover is induced by the unidirectional anisotropy arising from interparticle interaction, and this is confirmed from the presence of exchange bias phenomenon.

DOI: 10.1103/PhysRevB.82.094402 PACS number(s): 75.75.−c, 75.47.Lx, 75.40.Gb, 75.20.−g

I. INTRODUCTION

The complex coupling between spin, charge, orbital, and lattice in perovskite manganites around half doping gives rise to various exotic electromagnetic properties.[1–3] The critical balance between the competing antiferromagnetic (AF)—insulating (I), and ferromagnetic (FM)—metallic (M) orders is found to be rather susceptible to small perturbations which can cause drastic effects.[4,5] In the recent time, it is shown that the reduction in the particle size or dimensionality have rather significant effects on the physical properties. The charge-ordering (CO), orbital-ordering (OO), and low-temperature (T) AF states are largely modified in the thin films of $Nd_{0.5}Sr_{0.5}MnO_3$ and $Pr_{0.5}Sr_{0.5}MnO_3$.[6,7] In the parallel developments, it is demonstrated that in the nanoparticles, the notable bulk properties such as CO, OO, low-temperature AF states are largely suppressed or weakened, and the system emerges to FM state.[8–11] However, it was suggested by Néel long back that the small or finite-size particles of AF material should exhibit superparamagnetism (SPM) or weak FM properties.[12]

The physical properties in nanoparticles are mainly modified due to (i) the finite-size effect, and (ii) the surface disorder effect which is caused by defects, broken exchange bonds, fluctuations in number/separation of neighboring atoms at the surface, etc. Usually, FM particles with reduced size behave as a single domain entity exhibiting SPM behavior where the thermal fluctuation overcome the anisotropy energy of individual particle causing the magnetization to flip from one to another easy direction. The situation becomes complicated if there exists interparticle interactions which induces collective behavior and may modify the magnetic properties drastically. For instance, it is observed for ferrofluid that low-T dynamics changes from SPM to spin-glass (SG) like behavior with just increasing interaction among the particles.[13] Therefore, it is necessary to identify the nature as well as the extent of this interaction to characterize the magnetic properties of the collection or conglomerate of nanoparticles. Commonly, the interparticle interaction is achieved or modulated with the variation in volume concentration of particles, however, the size variation in particles offer another avenue in this regard which does not require the intervening materials unlike the former case, and is uncommon in literature.

Here we present a detailed study of the magnetic properties and their evolution with the interparticle interaction in nanoparticles of half-doped manganite, $Pr_{0.5}Sr_{0.5}MnO_3$ (PSMO). In this study, we have modulated the interparticle interaction by means of modifying the size of the particles. Nanoparticles of three different average sizes (in the range of 15–27 nm) are synthesized which have identical room-temperature crystal symmetry as their bulk counterpart. However, contrary to the bulk PSMO, these nanoparticles do not show the low-temperature FM to AF transition.[14,15] Using the linear and nonlinear ac susceptibility coupled with dc magnetization, we have confirmed that these nanoparticles show SPM behavior where the blocking temperature (T_B) increases with the particle size. Analysis of frequency-dependent peak in ac susceptibility and temperature variation in coercive field indicate the presence of interparticle interaction. The nature of the interaction is found to be of dipolar type and its strength decreases with increasing particle size. It is rather significant that with increasing the field (H), all the nanoparticles exhibit a crossover in critical lines from the de Almeida-Thouless (AT)- to the Gabay-Toulouse (GT)-type behavior around the respective dipolar interaction field. Following the theoretical prediction, we believe that this crossover is induced by unidirectional anisotropy which, in the present systems arises from the interparticle interaction and is confirmed from the presence of exchange bias effect.

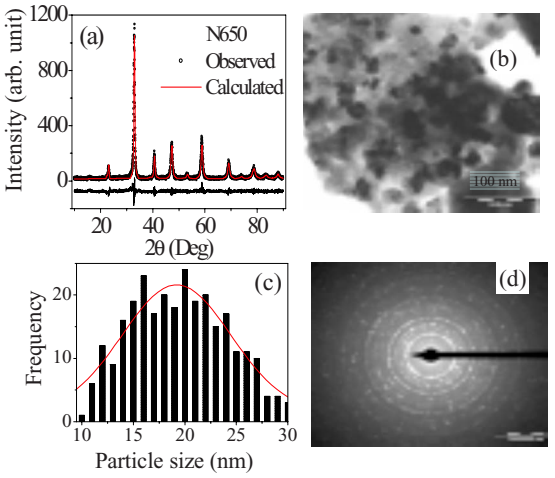

FIG. 1. (Color online) (a) Rietveld refinement profile of powder XRD pattern of N650 sample at room temperature. The open circles and solid continuous lines represent the observed and calculated pattern, respectively. The difference plot is shown at the bottom of the figure. (b) The bright-field TEM image of N650 sample collected at room temperature. (c) Histogram obtained from several TEM images shows particle size distribution for N650 sample. (d) Room-temperature selected-area electron-diffraction (SAED) pattern of N650 sample showing good crystalline nature of nanoparticles.

II. EXPERIMENTAL DETAILS

Nanocrystalline samples of PSMO are prepared, using Pr_6O_{11}, $SrCO_3$, and $Mn(CH_3COO)_2$ with purity of 99.99% or better by chemical (pyrophoric) method.[16] First, the proportional amount of ingredients are dissolved in dilute HNO_3. Triethanolamine (TEA) is mixed with this aqueous solution of the ingredients in the metal ions to TEA ratio as (Pr,Sr):Mn:TEA=1:1:4 and evaporated around 200 °C. At the end, it yields black precursor powders which are heated at 600, 650, and 700 °C for 5 h to get the powders of different nanosize samples which are designated as N600, N650, and N700, respectively. Room-temperature x-ray diffraction (XRD) patterns are collected with Rigaku Dmax 300 diffractometer attached to 18 kW rotating anode (Cu) source. Rietveld refinement[17] of XRD patterns show that samples are in single phase and they crystallize in tetragonal structure with $I4/mcm$ symmetry similar to their bulk counterpart. Figure 1(a) presents XRD data along with the Rietveld fitting for the N650 sample. Average particle size (D_{XRD}) has been estimated from the XRD plot using Scherrer formula.[18] The calculated particle sizes are given in Table I. Structural parameters found from the Rietveld refinements are also given in Table I. There is no major structural modification in nanometric samples compared to the bulk.[15] Extreme right column of Table I presents the percentage change in the related parameters for all the samples, showing that no major structural modification occurs with the size variation in particles.

Samples are also characterized through transmission electron microscope (TEM) (model: TECNAI G2–20FEI). Figure 1(b) shows TEM bright-field image of N650 sample. Histogram for particle size distribution is obtained after analyzing several TEM images. Such histogram for N650 sample, presented in Fig. 1(c), shows that particles are polydisperse in nature. Mean particle size (D_{TEM}) for all the samples have been obtained from the Gaussian fitting of figure similar to Fig. 1(c) and values are given in Table I. The values of D_{XRD} and D_{TEM} match reasonably well except for N700 sample. This mismatch in sizes for N700 may be arising from conglomeration of particles because of higher-temperature processing. Selected-area electron-diffraction (SAED) graph has been given in Fig. 1(d) for N650 sample. The figure shows well distinct spotty concentric ring indicating crystalline nanoparticles. The similar figure for N600 sample is given in Ref. 19. The oxygen stoichiometry or Mn^{3+}/Mn^{4+} ratio of 1:1 is ensured from Iodometric Redox titration. Low-field ac-susceptibility measurements are done with home made ac susceptometer.[20] The dc magnetization have been measured with homemade vibrating sample magnetometer (VSM) (Ref. 21) and commercial 14 T VSM physical proerty measurement system (PPMS) made by Quantum Design.

TABLE I. Structural parameters are determined from the Rietveld refinement of the powder XRD patterns for nanocrystalline $Pr_{0.5}Sr_{0.5}MnO_3$. Here O1 is the apical and O2 is the equatorial oxygen in perovskite structure. D_{XRD} and D_{TEM} are the average particle sizes calculated from the XRD and TEM measurements. T_B is the blocking temperature obtained from ac susceptibility. The extreme right column shows the percentage change (Δ%) in structural parameters for all the nanoparticles.

Samples	N600	N650	N700	Δ%
a (Å)	5.4270(7)	5.4259(5)	5.4255(5)	−0.02
c (Å)	7.7267(17)	7.7226(12)	7.7213(12)	−0.06
V (Å^3)	227.57(6)	227.35(5)	227.29(5)	−0.12
Mn-O1 (Å)	1.9317	1.9306	1.9303	−0.07
Mn-O1-Mn	180°	180°	180°	0.0
Mn-O2 (Å)	1.9337	1.9278	1.9303	−0.25
Mn-O2-Mn	165.7°	168.6°	167.1°	+1.7
D_{XRD} (nm)	15.7	17.3	19.1	
D_{TEM} (nm)	15.7	19.2	26.6	
T_B (K)	209.8	240.3	253.3	

III. RESULTS AND DISCUSSIONS

A. Superparamagnetic behavior of nanoparticles

Figure 2 presents the temperature variation in dc magnetization (M) measured in 100 Oe following zero-field-cooled (ZFC) and FC warming (FCW) protocols. ZFC magnetization shows broad peak at characteristic temperature (T_B) which is unlike its bulk compound where the sample exhibits clear PM-FM and then FM-AF transition on cooling from room temperature.[14,22] The observed peak which is typical feature of metastable magnetic systems such as SPM particles or SG system, shifts to higher T with increasing particle size. It is clear in figure that ZFC and FCW branches of magnetization split at temperature (T_{irr}) higher than T_B, and T_{irr} reduces with increasing the field (not shown). The higher

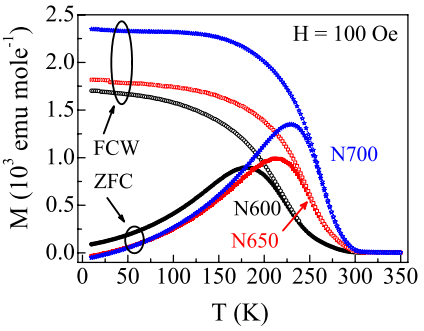

FIG. 2. (Color online) Temperature variation in dc magnetization collected in 100 Oe following ZFC and FCW protocols for all the nanoparticles.

value of T_{irr} than T_B indicates the presence of larger size spin clusters which are ordered at higher temperature. Contrary to the bulk PSMO, the first-order FM-AF transition at lower temperature as well as the associated hysteresis between FCW and the FC cooling magnetization, down to 2 K, is not evident in these nanoparticles. Similar phenomenon, however, is observed in various nanocrystalline half-doped manganites.[8–10] From the Curie-Weiss fitting of high-T magnetization data [$(\chi=M/H)^{-1}$ vs T], the effective PM moment (μ_{eff}) has been calculated in terms of Bohr magneton (μ_B) per formula unit (f.u.). The obtained values are 3.62, 3.70, and 4.38 μ_B/f.u. for N600, N650, and N700 compound, respectively. It can be noted that μ_{eff} for smaller particles are lower than the expected spin only value ($\mu_{eff}=g\sqrt{S(S+1)}$, where S is the total spin) which is 4.38 μ_B/f.u. for PSMO. It is noteworthy that with increasing particle size, μ_{eff} approaches the expected value.

To understand the low-T magnetic state in these nanoparticles we have collected high field (120 kOe) M vs H plots at 2 K [Fig. 3(a)]. Unlike the bulk PSMO which at low T (within AF state) exhibits field induced jump in $M(H)$ and attains the saturation moment (3.5 μ_B/f.u.),[15,23] the nature of $M(H)$ plots for nanoparticles resemble qualitatively with FM systems. However, even in high field, magnetization does not saturate but show monotonous increase. The obtained magnetic moments at 2 K and 120 kOe are 1.38, 1.40,

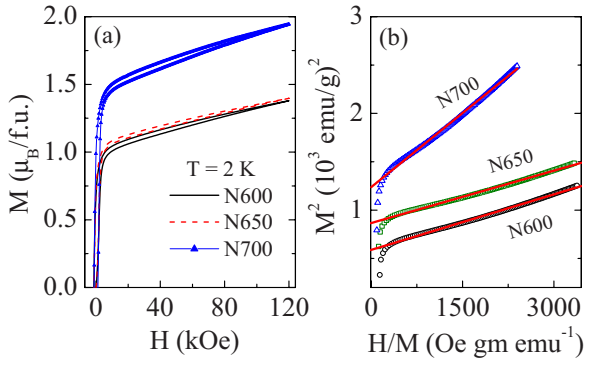

FIG. 3. (Color online) (a) Magnetization vs field data are shown for all the nanoparticles at 2 K. (b) Arrott plot (M^2 vs H/M) of the isotherms in (a) are shown. Lines are due to straight-line fitting of the plots in high fields. The data for N650 sample are vertically shifted by 200 for clarity.

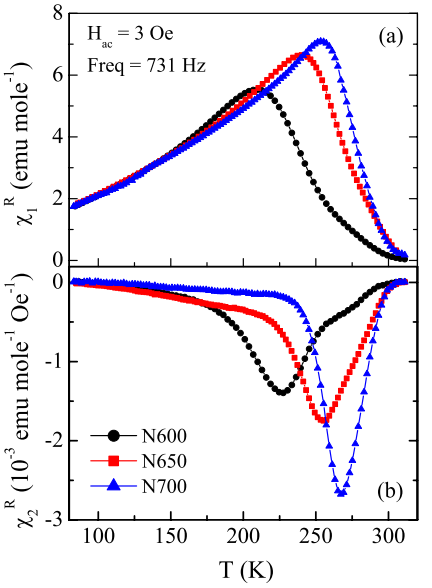

FIG. 4. (Color online) (a) Real part of first-order ac susceptibility measured in field 3 Oe and frequency 731 Hz are plotted as a function of temperature for all the nanoparticles. (b) Real part of second-order susceptibility is plotted as a function of temperature for all the nanoparticles in same field and frequency.

and 1.94 μ_B/f.u. for N600, N650, and N700 sample, respectively. These values are much lower than the saturation moment of bulk PSMO (3.5 μ_B/f.u.). Nonetheless, the estimated moments imply that the increased surface-to-volume ratio at smaller particles creates higher amount of magnetically dead layer at the surface, thus it reduces the average moment systematically. In Fig. 3(b), $M(H)$ data are plotted in the form of M^2 vs H/M which is known as Arrott plot.[24] Positive intercept on the M^2 axis from the extrapolation of high-field data in Arrott plot implies the presence of spontaneous magnetization in system. The spontaneous magnetization calculated from these intercepts [Fig. 3(b)] are 0.943, 1.003, and 1.367 μ_B/f.u. for N600, N650, and N700 sample, respectively. This clearly indicates that the ground state of these nanoparticles are FM contrary to their bulk counterpart even though there is no change in the structural symmetry.

To confirm the magnetic state of these nanoparticles we have measured ac susceptibility (χ) which probes the dynamics of the spin system in very low field. In general, magnetization can be expressed in terms of measuring field as

$$M = M_0 + \chi_1 H + \chi_2 H^2 + \chi_3 H^3 + \chi_4 H^4 + \cdots, \qquad (1)$$

where M_0 is the spontaneous magnetization, χ_1 is the linear and χ_2, χ_3, χ_4 are the nonlinear susceptibilities. Figure 4(a) presents temperature variation in real part of χ_1 (χ_1^R) measured in ac field 3 Oe and frequency 731 Hz. The feature of χ_1^R is similar to its dc magnetization counterpart presented in Fig. 2. The T_B calculated from low-field ac χ are mentioned in Table I.

It is rather nontrivial issue to distinguish between the SPM and SG as both share similar kind of experimental features. To do this, we have used nonlinear ac susceptibilities which are shown to be the useful experimental probes to

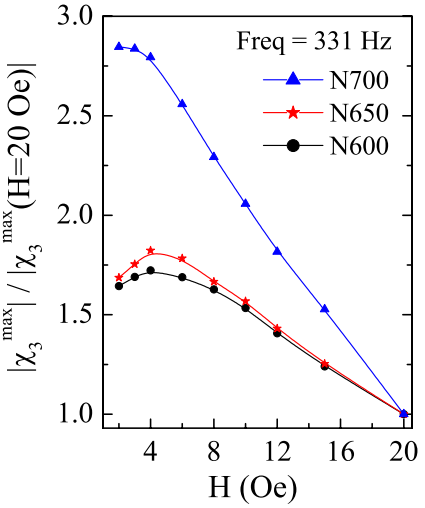

FIG. 5. (Color online) The maximum value of χ_3 normalized by that at 20 Oe has been plotted as a function of applied ac field for all the nanoparticles which clearly shows the nondiverging behavior of χ_3 as $H \rightarrow 0$.

separate out different magnetic states.[15,25–29] In Fig. 4(b), we have plotted temperature dependence of second-order ac χ (χ_2) measured in ac field 3 Oe and frequency 731 Hz. Usually, χ_2 appears due to the presence of symmetry-breaking field which originates either from the spontaneous magnetization or the superimposed dc magnetic field.[15,26,27] As the canonical SG does not hold spontaneous magnetization, so χ_2 should be absent without dc field. The presence of finite χ_2 in Fig. 4(b) confirms the presence of FM interaction within these nanoparticles and discards the possibility of canonical SG-like phase. However, it is important to identify if the broad peak in ZFC magnetization and in χ_1^R can be attributed to cluster-glass-like phase or SPM. This is achieved through the measurement of third-order ac χ [$\chi_3(T)$] which show broad negative peak around T_B for all the samples (not shown). The SPM-like feature in the present nanoparticles is confirmed from the noncritical behavior of the χ_3 around the peak temperature. It has been unambiguously shown that, for SG-like system, χ_3 diverges as $H \rightarrow 0$ around the transition temperature.[25,30] In Fig. 5, we have plotted the maximum value of χ_3 normalized by that at $H=20$ Oe as a function of measuring field. As evident in figure, χ_3 is not divergent as $H \rightarrow 0$. This analysis shows conclusively that PSMO nanoparticles do not show SG-like cooperative freezing but thermal blocking of the magnetic entities.

Further, the SPM behavior in these nanoparticles is also substantiated from the Wohlfarth's model.[28,31] The magnetization for an assembly of particles is given as

$$M = n\langle\mu\rangle L(\langle\mu\rangle H/k_B T), \tag{2}$$

where n is the number of particles per unit volume, $\langle\mu\rangle$ is the average moment of magnetic particle, k_B is the Boltzmann constant, and $L(x)$ is the Langevin function. After the expansion of $L(x)$, χ_1 and χ_3 above the blocking temperature (T_B) can be expressed as

$$\chi_1 = n\langle\mu\rangle^2/3k_B T = P_1/T, \tag{3}$$

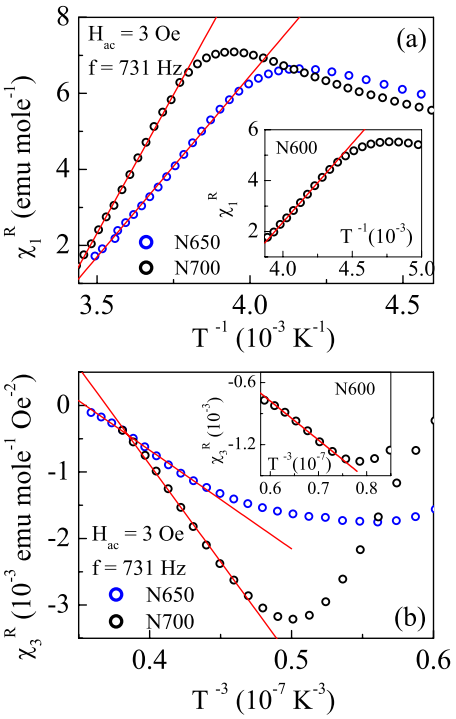

FIG. 6. (Color online) Temperature variation in (a) first-order and (b) third-order ac susceptibility is plotted above the blocking temperature for N650 and N700 samples. Straight lines are the (a) T^{-1} fit to χ_1 [Eq. (3)] and (b) T^{-3} fit to χ_3 [Eq. (4)] data. Inset shows the same plotting for N600 sample in the respective graphs.

$$\chi_3 = (n\langle\mu\rangle/45)(\langle\mu\rangle/k_B T)^3 = P_3/T^3. \tag{4}$$

Therefore, χ_1 and χ_3 above T_B for SPM will vary as T^{-1} and T^{-3}, respectively. The main panels of Figs. 6(a) and 6(b) show this variation in χ_1^R and χ_3^R following Eqs. (3) and (4), respectively, for N650 and N700 samples. In the inset of both the figures we show the same plot for N600 sample. This further corroborates the earlier analysis that peak in χ_1 arises due to the blocking of magnetic clusters in the present study. From the ratio of P_3 and P_1, $\langle\mu\rangle$ is estimated which are around 14.5×10^4, 22.9×10^4, and 26.1×10^4 μ_B for N600, N650, and N700 sample, respectively. This large value of $\langle\mu\rangle$ is consistent with the SPM clusters as it consists of large number of spins, whereas for PM, $\langle\mu\rangle$ signifies only ionic moments and is limited to few μ_B. Assuming that clusters are spherical, effective sizes of them are calculated from the values of $\langle\mu\rangle$ derived from above analysis. These sizes are found to be around 16.5, 19.2, and 20.9 nm for N600, N650, and N700, respectively. It is noteworthy that effective size of clusters calculated from the magnetic measurement are close to the same obtained from XRD and TEM measurements (Table I). This consistency of particle size calculated from various methods proves the unambiguity in present analysis.

B. Interaction among the nanoparticles

After having confirmed the SPM nature of these nanoparticles, we attempt to establish the existence of interparticle interaction. As a first step, interparticle interaction is identified from the temperature dependence of coercive field (H_C)

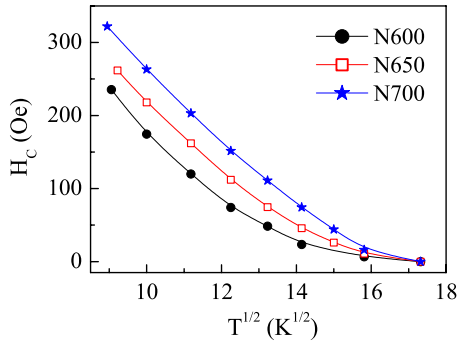

FIG. 7. (Color online) Temperature dependence of coercive fields for all the samples.

estimated from the $M(H)$ plot for all the samples. For the noninteracting SPM particles, temperature variation in H_C is expressed as[32]

$$H_C = H_{C,0}[(1 - T/T_B)^{1/2}], \tag{5}$$

where $H_{C,0}$ is the value of H_C when $T \to 0$. Thus, the measured H_C as a function of $T^{1/2}$ would be linear for noninteracting particle systems. However, nonlinear behavior of H_C vs $T^{1/2}$ in Fig. 7 arises due to the interaction among the particles. It is also evident in the figure that with increasing particle size the nonlinearity in plot is reduced, thus probably indicate that the strength of interaction reduces with the increasing particle size.

Now we attempt to reestablish the presence of interaction among the particles from the frequency (f) dependent shift in T_B in ac-$\chi(T)$ measurements. It can be mentioned that the variation in f in ac χ renders the variation in probe time $\tau_P(\propto f^{-1})$ which allows to probe the relaxation of particles in different time windows. It is observed in Fig. 8 that χ_1^R for N600 sample decreases and T_B shifts toward higher T with increasing f. However, the shift of T_B with the f in present study is relatively small. It can be mentioned that simple, noninteracting SPM particles show large f dependence of T_B whereas for SG or interacting SPM particles, T_B is less f dependent.[33] The f dependence of T_B is normally quantified with the following empirical relation:

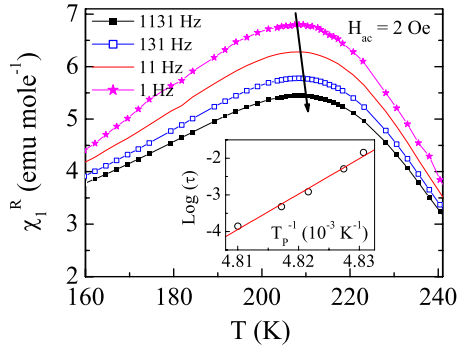

FIG. 8. (Color online) Temperature dependence of real part of χ_1 at various frequencies is plotted for N600 compound. Arrow indicates peak shift with the increasing frequencies. Inset shows Néel-Arrhennius law [Eq. (6)] fitting of frequency-dependent peak temperature (defined in text).

$$\Phi = \frac{\Delta T_B}{T_B \Delta \log_{10}(f)}, \tag{6}$$

where Δ is the difference in related parameters. The value of Φ for N600 sample is found to be around 0.002. The other two samples also show similar values of Φ. The experimentally determined values of Φ for SPM particles are in the range of 0.1–0.13, whereas much lower values (0.005–0.05) are observed for canonical SG systems as well as interacting particle system.[34,35] Therefore, based on the value of Φ it is often difficult to distinguish between SPM and SG experimentally. However, the calculated Φ hints toward the presence of interaction among these particles.

To unambiguously identify the presence of interparticle interaction, we follow a rigorous systematic method where the f dependence of T_B has been analyzed with different phenomenological models. According to Néel-Arrhennius law, relaxation time (τ) for an assembly of noninteracting SPM particles behaves like[36]

$$\tau = \tau_0 \exp\left(\frac{E_a}{k_B T}\right). \tag{7}$$

E_a is the anisotropy energy barrier equal to KV, where K is the anisotropy energy constant and V is the volume of the particles. For the SPM relaxation, the prefactor τ_0 is in the range of 10^{-8}–10^{-13} s.[37] Inset of Fig. 8 shows the straight line fitting of Eq. (6) for N600 sample. Though fit is apparently good but the obtained values are quite unphysical ($\tau_0 \approx 10^{-522}$ and $E_a/k_B = 253\,615$) which clearly indicates that dynamics of these nanoparticles cannot be explained with noninteracting particle model. Thus, we have tried to analyze the f-dependent shift of T_B using Vogel-Fulcher law,[36]

$$\tau = \tau_0 \exp\left[\frac{E_a}{k_B(T - T_0)}\right]. \tag{8}$$

The term T_0 is the characteristic temperature ($0 < T_0 < T_B$) which accounts the interaction among the particles. In this case, best fitting of data for N600 has been shown in Fig. 9(a). The obtained fitted parameters are quite reasonable with the values $E_a/k_B = 25.27 \pm 3.34$ K, $T_0 = 205.15$ K, and $\tau_0 = 1.76 \times 10^{-8}$ s. Such higher value of τ_0 has been observed for interacting clusters.[38] This fitting confirms the interacting nature of these nanoparticles and is in conformity with the recent observations such as slow magnetic relaxation with logarithmic time dependence and memory effects.[19]

It is rather significant and intriguing that the f-dependent shift of T_B can be fitted to the scaling law as well, which is used to characterize the phase transition in SG, though the present system are proved to be almost tailor-made small particles, which behave like SPM beyond doubt. The scaling hypothesis assumes that the relaxation time (τ) is related to the correlation length (ξ) near to the transition temperature (T_g). As ξ diverges at T_g, relaxation time obeys the following empirical relation:[36]

$$\tau = \tau_0 (T/T_g - 1)^{-z\nu}, \tag{9}$$

where z is the dynamical scaling exponent and ν is the critical exponent related to ξ. Figure 9(b) shows the best fit of

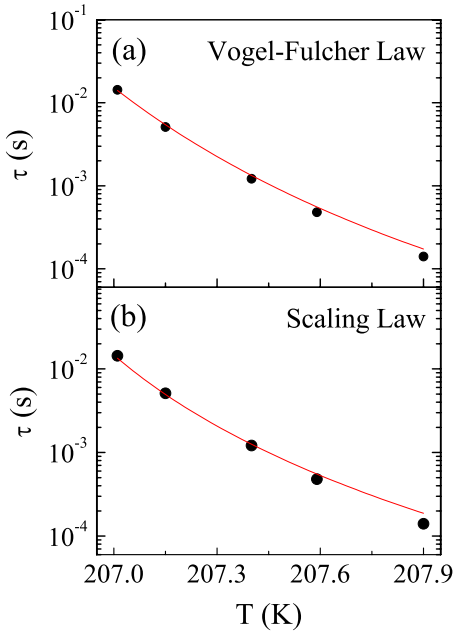

FIG. 9. (Color online) The best fit of the relaxation times (τ) to (a) the Vogel-Fulcher law [Eq. (7)] and (b) the scaling law [Eq. (8)] for N600 sample.

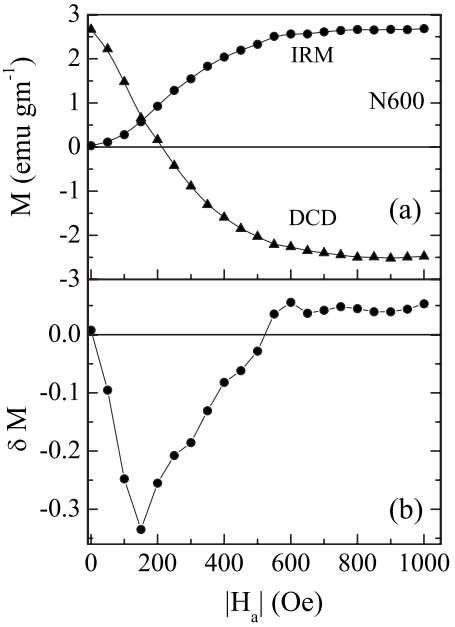

FIG. 10. (a) Remnant magnetization measured following IRM and DCD protocols (defined in text) are plotted as a function of applied field for N600 sample. Bottom panel shows calculated δM values following Eq. (10) for the same sample.

Eq. (8) for N600 sample and the obtained parameters are $\tau_0 = 3.39 \times 10^{-14}$ s, $T_g = 206.44$ K, and $z\nu = 4.52$. Usually, the exponent $z\nu$ shows large variation for different kind of systems.[39] The obtained $z\nu$ is close to the theoretically predicted value (4) for three-dimensional Ising model,[40] and the experimentally calculated value (5.5) for canonical SG $CuMn_{4.6\%}$.[39] However, τ_0 shows large disagreement between Vogel-Fulcher law and scaling law fitting. Further, τ_0 obtained in later case is orders of magnitude less than that usually seen for SG (10^{-11}–10^{-12} s). This inconsistency of τ_0 with that for SG is rather significant, which discards the possibility of SG-like freezing in these nanoparticles.[36] It is fact that the significant presence of interparticle interaction induces the collective behavior and glassy dynamics even in the tailor made SPM system. Since the response of such systems is similar to SG, they are termed as super SG (SSG).[13,38,41,42] Basically, SSG dynamics differ from the SPM one in terms of critical slowing down of relaxation time. Similar critically slow dynamics resembling SG-like response is also shown by magnetic clusters forming in a matrix out of composition fluctuation or atomic segregation which is called cluster glass (CG).[43] However, it remains an experimentally challenging task to discern between critically slow dynamics of SSG and CG with the slow but noncritical dynamics of SPM system. The high value of τ_0 and T_0 obtained from the Vogel-Fulcher law fitting unambiguously imply the presence of interparticle interaction in present nanoparticles,[33] however, the obtained τ_0 from the dynamical scaling hypothesis fitting is a few orders lower than the value for SSG or CG ($\tau_0 = 10^{-9}$–10^{-6}).[13,38,41,42] Nonetheless, the fitting of scaling law for our data is quite intriguing indicating some sort of glassiness in the system, however, the overall results do not comply with the SSG behavior. This indicates that a careful exercise is needed to make a proper distinction between the SSG/CG-like phases with that of SPM system from the dynamical behavior.

C. Nature of interparticle interaction and its consequences on magnetic properties

To identify the nature of the interparticle interaction and its consequences on the magnetic properties, we have measured the remnant magnetization following isothermal remnant magnetization (IRM) and dc demagnetization (DCD) protocols.[44] For the IRM measurement, we cooled the sample in zero field from the room temperature to 150 K and applied a field (H_a) isothermally for 10 s. Then the H_a is reduced to zero and remnant magnetization is measured. We heated the sample back to room temperature and repeated this experiment for different H_a at the same temperature, each time increasing H_a in steps of 50 Oe up to maximum of 1000 Oe. The measured IRM as function of H_a for N600 sample is depicted in Fig. 10(a). In DCD measurement, the sample is zero-field cooled from room temperature to 150 K and magnetized to saturated state with applying +1000 Oe for 10 s. The applied positive field is made zero and isothermally a negative field ($-H_a$) is applied for 10 s. Then, $-H_a$ is switched off and remnant magnetization is measured. We repeated this experiment similar to IRM measurement for different $-H_a$ up to -1000 Oe in step of -50 Oe. The measured DCD as function of $|H_a|$ for N600 sample is depicted in Fig. 10(a). It can be mentioned that IRM and DCD originate from the virgin and saturated state, respectively.

To characterize as well as quantify the magnetic interaction, the parameter δM is shown to be very useful which is defined as[44,45]

$$\delta M = m_{\mathrm{DCD}} - (1 - 2m_{\mathrm{IRM}}), \tag{10}$$

where m is the normalized remnant magnetization with respect to the remnant magnetization measured after the

sample is magnetized to saturated state. For noninteracting particles δM is zero.[45] However, finite interactions among the particles lead to deviation of δM from zero, i.e., positive δM is due to the interactions which favor magnetization whereas negative δM arises from the interactions which cause demagnetization in the system.[44] Usually, the negative δM implies the dipolar interaction and the field where minimum in δM occurs quantifies the strength of interaction.[46] We have plotted δM as a function of $|H_a|$ for N600 sample in Fig. 10(b). As evident in figure, δM is negative in low H_a, showing minimum around 150 Oe. In higher H_a around 522 Oe, δM shows crossover to positive value. We can infer from this results that interparticle interaction is of *dipolar* type, having magnitude roughly of 150 Oe. At high field, interparticle interaction is dominated by the applied field yielding positive δM. For the same measurements on N700 compound, δM shows negative minimum around 100 Oe, and crossover to positive value around 220 Oe. These results indicate that with the increasing particle size, strength of dipolar interaction reduces. The dipolar interaction between two magnetic dipoles $\vec{\mu}_i$ and $\vec{\mu}_j$ can be estimated as[36]

$$E_d = \frac{1}{r_{ij}^3}[\vec{\mu}_i \cdot \vec{\mu}_j - 3(\vec{\mu}_i \cdot \hat{r}_{ij})(\vec{\mu}_j \cdot \hat{r}_{ij})], \tag{11}$$

where r_{ij} is the center-to-center distance between the dipoles. Equation (11) gives the form of long-range dipolar interaction energy between the two magnetic diploes of moment $\langle\mu\rangle$ separated by distance r_{ij}. For a collection of small particles, it has to be summed over all the particles. The present system may be considered as an assembly of spherical nanoparticles of radius R, placed adjacent to each other in a regular array. In this case, the separation between the adjacent magnetic moments, r_{ij}, is about $2R$. If we consider the magnetic moment $\langle\mu\rangle$ of each particle is roughly proportional to its volume, then according to Eq. (11), dipolar interaction energy (E_d) between the two adjacent particles varies approximately as R^3. Since for a collection of particles within a given volume, the number of particles varies as inverse of R^3, the total interaction energy which is the summation over the entire individual E_d's, becomes almost independent of the particle size. However, in real situation, as the average particle size decreases, the packing fraction increases in such densely packed assembly of nanoparticles having a distribution in particle size. Thus decrease in the size will result in the increase in the number of particles in the same volume, much more than what is expected for a regular array where it increases as $1/R^3$. Moreover, for such dense packing, reduction in the size of the particles will also reduce the average distance between them, r_{ij}, faster than a linear function of R. Both this factors will contribute to increase the total dipolar interaction energy in the system with the decrease in particle size. The evidence of such increase in dipolar interaction energy with the decrease in the particle size in the present system can be found in the Fig. 7 and the discussions of Secs. III B and III C.

The dipolar interaction has significant influences on the magnetic properties as it modifies the otherwise uniaxial anisotropy energy barrier of individual nanoparticle. The most notable effects of this interaction are the evolution of glassy dynamics,[13] modification in T_B,[13,47] etc. Here we have looked into the effect of dipolar interaction on the field dependence of T_B by measuring ZFC magnetization in different fields. In the experimental scenario, T_B corresponds to the temperature where τ_P equals to the average τ of the system. Since with the variation in applied field T_B varies, thus one can construct a line of constant τ on the plane spanned by H and T. The existence of such line is predicted in the mean-field theoretical model for SG. To be specific, this model assumes phase transition in SG, and considers that large field will destroy the frozen spin state.[36] Therefore, in presence of field, the critical lines are predicted on the H-T plane which mark the phase transition. The first one is the de Almeida-Thouless (AT) line occurring in anisotropic Ising SG and behaves as $T_B(H) \propto H^{2/3}$. The second one is the Gabay-Toulouse (GT) line valid for isotropic Heisenberg case and shows functional form $T_B(H) \propto H^2$.[36] However, later numerical calculation showed that such lines are not unique for SG and can even exist in case of relaxation of (interactive) SPM particles with the crossover from low-H GT to high-H AT behavior.[48] Our results are plotted in Fig. 11 where we show that variation in T_B with field follows AT line in low field for all the samples. However, with the increase in field we find the deviation from AT line as marked by vertical arrows in the figure. Remarkably, in high field we find the variation in $T_B(H)$ agrees with the GT line. We have observed the similar behavior for all the samples and in inset of Fig. 11 we have plotted such high-field behavior for N600 sample. The fields (H_{cr}) where we find crossover from AT to GT behavior are approximately 250, 200, and 100 Oe for N600, N650, and N700 sample, respectively. It is rather significant that the crossover fields from AT to GT like behavior are close to the dipolar interaction fields found from the remnant magnetization measurements mentioned above (Fig. 10). This crossover in critical lines around the dipolar interaction field for these nanoparticles is quite noteworthy.

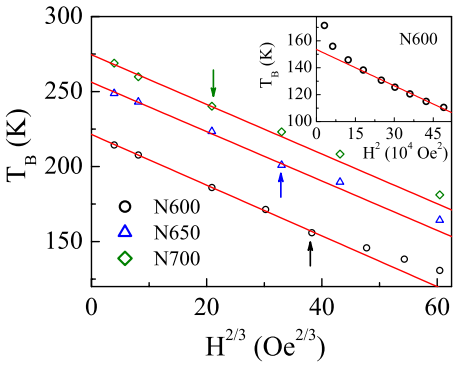

FIG. 11. (Color online) The temperatures where the peak occurs in ZFC magnetization are plotted as a function of applied field for all the samples. Straight line is fit to AT line (defined in text). The vertical arrows mark the field above which systems deviate from AT line behavior. Inset: field dependence of peak temperature has been fitted to GT line for N600 sample (defined in text).

The above experimental results in Fig. 11 has the similarity with the theoretical calculation by Kotliar and Sompolinsky[49] who predicted that in presence of unidirec-

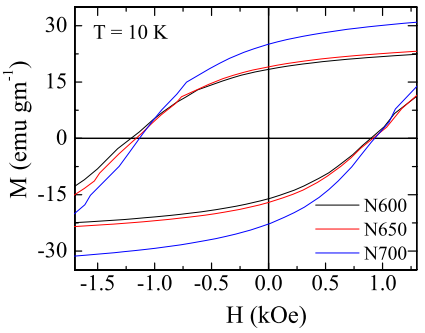

FIG. 12. (Color online) Field-cooled M vs H loops collected after cooling the samples in 10 kOe from room temperature to 10 K. The recorded loops exhibit shift along the field axis toward negative direction.

tional random anisotropy (i.e., Dzyaloshinsky-Moriya-type interaction) the critical behavior for SG in fields lower than the anisotropy is close to Ising-type following AT line, and crosses over to Heisenberg behavior in high fields. In fact, similar anisotropy induced crossover in critical lines is experimentally observed in Au-doped classical CuMn SG system as well as in superconducting vortex-glass system.[50,51] These results allow us to draw an analogy with the present PSMO nanoparticles where the interparticle interaction acts as an unidirectional anisotropy leading to crossover from AT to GT like behavior at field around the interaction field. Indeed, dipolar interaction [Eq. (11)] is anisotropic which introduces angular dependence of spin ordering in system.[36]

To confirm the unidirectional nature of the anisotropy arising out of interparticle interaction we have measured FC M vs H loop for all the nanoparticles. In presence of unidirectional anisotropy, FC hysteresis loop is shifted along the field axis, generally, in opposite direction to the cooling field. This loop shift is commonly known as "exchange bias (EB)" which is characterized by field, H_E.[52] The samples under study have been cooled in +10 kOe from room temperature to 10 K and after proper thermal stabilization hysteresis loops have been recorded (Fig. 12). We have ensured that the artifacts due to minor hysteresis loop are eliminated. It is evident in figure that collected M vs H loop is shifted toward the negative field axis. It is worth mentioning that we find similar opposite shift when samples are cooled in negative field. We calculate H_E [$=-(h_+-h_-)/2$, where h_- and h_+ are the point of intersection on the field axis at decreasing (−) and increasing (+) fields cycles] as 155.3, 132.4, and 105.7 Oe at 10 K for N600, N650, and N700 sample, respectively. Conventionally, EB is believed to be directly associated with the interface of FM and AF components. However, FM in contact with SG or ferrimagnets are also observed to give rise EB properties.[52,53] For the present PSMO nanoparticles, we believe that the observed EB is guided by the interparticle interaction rather than the FM/AF interface mechanism. Our conclusion is based on the following points: (i) Fig. 3 conclusively shows the FM nature of low-T magnetic state for all the nanoparticles. (ii) Even if, EB arises due to the presence of residual AF components then H_E would vanish above the FM-AF phase transition temperature T_N. We find finite H_E at or above 150 K whereas T_N during cooling in same field occurs around 84 K for bulk PSMO.[22] (iii) The residual AF components are supposed to increase with the increasing particle size as the decrease in particle size does not favor AF ordering,[8,10] therefore it will result in more FM/AF interfaces. But, our estimated H_E decreases with increasing particle size. (iv) The variation in H_E follows the similar trend of interparticle interaction, i.e., decreases with increasing particle size. These results straightforwardly imply that EB in these PSMO nanoparticles originate due to the mechanism guided by the interparticle interaction. Furthermore, these confirm the unidirectional-anisotropic nature of this interparticle interaction which leads to crossover in critical lines on the H-T plane. Details of EB in these nanoparticles will be published elsewhere. Nonetheless, this interparticle interaction induced crossover in critical lines with fields in these compounds is quite intriguing and requires further studies involving both experimental and theoretical endeavor to comprehend.

IV. CONCLUSION

In conclusion, we show that nanoparticles of $Pr_{0.5}Sr_{0.5}MnO_3$ of three different average sizes have FM ground state contrary to their bulk counterpart in spite of having same crystallographic symmetry. The low-temperature FM-AF transition which is a marked feature of bulk compound is significantly absent in nanoparticles. Detailed linear as well as nonlinear ac susceptibilities coupled with dc magnetization confirm the SPM nature of these nanoparticles. Presence of interactions among these particles has been corroborated from the analysis of frequency-dependent peak in ac susceptibility and temperature dependence of coercive field. The nature of this interaction is identified to be of dipolar type and the strength of the interaction is found to decreases with the increase in particle size. This interparticle interaction gives rise to some kind of glassiness in the magnetic response even in these SPM system. The effect of this dipolar interaction on the magnetic properties is clearly evident as the systems exhibit crossover from AT- to GT-type critical lines with increasing field above their respective interaction field, which is rather intriguing. Following the theoretical prediction, we believe that this crossover phenomenon is induced by the presence of unidirectional anisotropy which arises from the interparticle interaction and the presence of exchange-bias effect in these samples confirms it.

ACKNOWLEDGMENTS

We are thankful to P. Chaddah for useful discussions. We acknowledge N. P. Lalla for XRD and TEM measurements. We also thank P. Dey for the help in sample preparation and Kranti Kumar for the help in measurements. DST, Government of India is acknowledged for funding VSM. A.K.P. also acknowledges CSIR, India for financial assistance.

*Present address: Leibniz Institute for Solid State and Materials Research (IFW) Dresden, D-01171 Dresden, Germany.

[1] C. N. R. Rao and B. Raveau, *Colossal Magnetoresistence, Charge Ordering and Related Properties* (World Scientific, Singapore, 1998).
[2] E. Dagotto, *Nanoscale Phase Separation and Colossal Magnetoresistance*, Springer Series in Solid State Sciences Vol. 136 (Springer, Berlin, 2002).
[3] Y. Tokura, Rep. Prog. Phys. **69**, 797 (2006).
[4] A. Banerjee, K. Mukherjee, K. Kumar, and P. Chaddah, Phys. Rev. B **74**, 224445 (2006).
[5] X. Chen, S. Dong, K. Wang, J.-M. Liu, and E. Dagotto, Phys. Rev. B **79**, 024410 (2009).
[6] Y. Wakabayashi, D. Bizen, H. Nakao, Y. Murakami, M. Nakamura, Y. Ogimoto, K. Miyano, and H. Sawa, Phys. Rev. Lett. **96**, 017202 (2006).
[7] Y. Uozu, Y. Wakabayashi, Y. Ogimoto, N. Takabo, H. Tamaru, N. Nagaosa, and K. Miyano, Phys. Rev. Lett. **97**, 037202 (2006).
[8] S. S. Rao, K. N. Anuradha, S. Sarangi, and S. V. Bhat, Appl. Phys. Lett. **87**, 182503 (2005); S. S. Rao and S. V. Bhat, J. Phys.: Condens. Matter **22**, 116004 (2010).
[9] A. Biswas, I. Das, and C. Majumdar, J. Appl. Phys. **98**, 124310 (2005).
[10] T. Sarkar, B. Ghosh, A. K. Raychaudhuri, and T. Chatterji, Phys. Rev. B **77**, 235112 (2008).
[11] Z. Jirák, E. Hadová, O. Kaman, K. Knížek, M. Maryško, and E. Pollert, Phys. Rev. B **81**, 024403 (2010).
[12] L. Néel, in *Low Temperature Physics*, edited by C. Dewitt, B. Dreyfus, and P. D. de Gennes (Gordon and Beach, New York, 1962), p. 413.
[13] T. Jonsson, J. Mattsson, C. Djurberg, F. A. Khan, P. Nordblad, and P. Svedlindh, Phys. Rev. Lett. **75**, 4138 (1995).
[14] Y. Tomioka, A. Asamitsu, Y. Moritomo, H. Kuwahara, and Y. Tokura, Phys. Rev. Lett. **74**, 5108 (1995).
[15] A. K. Pramanik and A. Banerjee, J. Phys.: Condens. Matter **20**, 275207 (2008).
[16] R. K. Pati, J. C. Ray, and P. Pramanik, J. Am. Ceram. Soc. **84**, 2849 (2001).
[17] R. A. Young, A. Sakthivel, T. S. Moss, and C. O. Paiva-Santos, *Users Guide to Program DBWS-9411* (Georgia Institute of Technology, Atlanta, 1994).
[18] B. D. Cullity, *Elements of X-Ray Diffraction* (Addison-Wesley, Philippines, 1956), p. 102.
[19] A. K. Pramanik and A. Banerjee, J. Phys.: Conf. Ser. **200**, 072075 (2010).
[20] A. Bajpai and A. Banerjee, Rev. Sci. Instrum. **68**, 4075 (1997).
[21] R. V. Krishnan and A. Banerjee, Rev. Sci. Instrum. **70**, 85 (1999).
[22] A. K. Pramanik and A. Banerjee, Phys. Rev. B **79**, 214426 (2009).
[23] A. Banerjee A. K. Pramanik, K. Kumar, and P. Chaddah, J. Phys.: Condens. Matter **18**, L605 (2006).
[24] A. Arrott, Phys. Rev. **108**, 1394 (1957).
[25] A. Bajpai and A. Banerjee, Phys. Rev. B **55**, 12439 (1997); **62**, 8996 (2000); J. Phys.: Condens. Matter **13**, 637 (2001).
[26] G. Sinha and A. K. Majumdar, J. Magn. Magn. Mater. **185**, 18 (1998).
[27] A. Chakravarti, R. Ranganathan, and C. Bansal, Solid State Commun. **82**, 591 (1992).
[28] T. Bitoh, K. Ohba, M. Takamatsu, T. Shirane, and S. Chikazawa, J. Magn. Magn. Mater. **154**, 59 (1996).
[29] S. Nair and A. Banerjee, Phys. Rev. Lett. **93**, 117204 (2004).
[30] M. Suzuki, Prog. Theor. Phys. **58**, 1151 (1977).
[31] E. P. Wohlfarth, Phys. Lett. A **70**, 489 (1979).
[32] B. D. Cullity, *Introduction to Magnetic Materials* (Addison-Wesley, Philippines, 1972), Chap. 11.
[33] J.-L. Tholence, in *Magnetic Susceptibility of Superconductors and Other Spin Systems*, edited by R. A. Hein, T. L. Francavilla, and D. H. Liebenberg (Plenum Press, New York, 1991), p. 503.
[34] G. F. Goya and V. Sagredo, Phys. Rev. B **64**, 235208 (2001).
[35] J. A. De Toro, M. A. López de la Torre, M. A. Arranz, J. M. Riveiro, J. L. Martínez, P. Palade, and G. Filoti, Phys. Rev. B **64**, 094438 (2001).
[36] K. Binder and A. P. Young, Rev. Mod. Phys. **58**, 801 (1986).
[37] J. L. Dormann, D. Fiorani, and E. Tronc, J. Magn. Magn. Mater. **202**, 251 (1999).
[38] C. Djurberg, P. Svedlindh, P. Nordblad, M. F. Hansen, F. Bodker, and S. Morup, Phys. Rev. Lett. **79**, 5154 (1997).
[39] J. Souletie and J. L. Tholence, Phys. Rev. B **32**, 516 (1985).
[40] K. Binder and A. P. Young, Phys. Rev. B **29**, 2864 (1984).
[41] X. Chen, S. Bedanta, O. Petracic, W. Kleemann, S. Sahoo, S. Cardoso, and P. P. Freitas, Phys. Rev. B **72**, 214436 (2005).
[42] M. Suzuki, S. I. Fullem, I. S. Suzuki, L. Wang, and C.-J. Zhong, Phys. Rev. B **79**, 024418 (2009).
[43] G. R. Gruzalski and D. J. Sellmyer, Phys. Rev. B **20**, 184 (1979).
[44] A. Butera, J. L. Weston, and J. A. Barnard, J. Appl. Phys. **81**, 7432 (1997).
[45] E. P. Wohlfarth, J. Appl. Phys. **29**, 595 (1958).
[46] J. Curiale, R. D. Sánchez, H. E. Troiani, C. A. Ramos, and H. Pastoriza, Phys. Rev. B **75**, 224410 (2007).
[47] S. Mørup and E. Tronc, Phys. Rev. Lett. **72**, 3278 (1994).
[48] L. E. Wenger and J. A. Mydosh, Phys. Rev. B **29**, 4156 (1984).
[49] G. Kotliar and H. Sompolinshy, Phys. Rev. Lett. **53**, 1751 (1984).
[50] N. de Courtenay, A. Fert, and I. A. Campbell, Phys. Rev. B **30**, 6791 (1984).
[51] P. Rodrigues, Jr., J. Schaf, and P. Pureur, Phys. Rev. B **49**, 15292 (1994).
[52] J. Nogués and I. K. Schuller, J. Magn. Magn. Mater. **192**, 203 (1999).
[53] M. Ali, P. Adie, C. H. Marrows, D. Greig, B. J. Hickey, and R. L. Stamps, Nature Mater. **6**, 70 (2007).